Research Article | Vol. 25, No. 19 | 18 Sep 2017 | OPTICS EXPRESS 22219
Optics EXPRESS

Nonlinear beam self-cleaning in a coupled cavity composite laser based on multimode fiber

R. GUENARD,[1] K. KRUPA,[1,2] R. DUPIOL,[2] M. FABERT,[1] A. BENDAHMANE,[2] V. KERMENE,[1] A. DESFARGES-BERTHELEMOT,[1] J. L. AUGUSTE,[1] A. TONELLO,[1] A. BARTHÉLÉMY,[1] G. MILLOT,[2] S. WABNITZ,[3,4] AND V. COUDERC[1,*]

[1]*Université de Limoges, XLIM, UMR CNRS 7252, 123 Avenue A. Thomas, 87060 Limoges, France*
[2]*Université de Bourgogne Franche-Comté, ICB, UMR CNRS 6303, 9 Av. A. Savary, 21078 Dijon, France*
[3]*Dipartimento di Ingegneria dell'Informazione, Università di Brescia, and INO-CNR, via Branze 38, 25123 Brescia, Italy*
[4]*Novosibirsk State University, 1 Pirogova str., Novosibirsk 630090, Russia*
[*]*vincent.couderc@xlim.fr*

Abstract: We study a coupled cavity laser configuration where a passively Q-switched Nd:YAG microchip laser is combined with an extended cavity, including a doped multimode fiber. For appropriate coupling levels with the extended cavity, we observed that beam self-cleaning was induced in the multimode fiber thanks to nonlinear modal coupling, leading to a quasi-single mode laser output. In the regime of beam self-cleaning, laser pulse duration was reduced from 525 to 225 ps. We also observed a Q-switched mode-locked operation, where spatial self-cleaning was accompanied by far-detuned nonlinear frequency conversion in the active multimode fiber.

OCIS codes: (140.3410) Laser resonators; (060.4370) Nonlinear optics, fibers; (060.3510) Lasers, fiber; (060.2320) Fiber optics amplifiers and oscillators; (190.3270) Kerr effect; (190.4223) Nonlinear wave mixing.

References and links

1. J. P. Koplow, D. A. V. Kliner, and L. Goldberg, "Single-mode operation of a coiled multimode fiber amplifier," Opt. Lett. **25**(7), 442–444 (2000).
2. J. R. Marciante, "Gain filtering for single-spatial-mode operation of large-mode-area fiber amplifiers," IEEE J. Sel. Top. Quantum Electron. **15**(1), 30–36 (2009).
3. S. H. Baek and W. B. Roh, "Single-mode Raman fiber laser based on a multimode fiber," Opt. Lett. **29**(2), 153–155 (2004).
4. J. Limpert, H. Zellmer, A. Tünnermann, T. Pertsch, and F. Lederer, "Suppression of higher order modes in a multimode fiber amplifier using efficient gain-loss-management (GLM)," in *Advanced Solid-State Lasers*, (Optical Society of America, 2002), paper MB20.
5. P. Steinvurzel, B. Kuhlmey, T. White, M. Steel, C. de Sterke, and B. Eggleton, "Long wavelength anti-resonant guidance in high index inclusion microstructured fibers," Opt. Express **12**(22), 5424–5433 (2004).
6. T. Bhutta, J. I. Mackenzie, D. P. Shepherd, and R. J. Beach, "Spatial dopant profiles for transverse-mode selection in multimode waveguides," J. Opt. Soc. Am. B **19**(7), 1539–1543 (2002).
7. H. S. Kim and M. C. Richardson, "Output characteristic of a gain guided, index anti-guided fiber amplifier under the condition of gain saturation," Opt. Express **17**(18), 15969–15974 (2009).
8. R. Florentin, V. Kermene, J. Benoist, A. Desfarges-Berthelemot, D. Pagnoux, A. Barthélémy, and J.-P. Huignard, "Shaping the light amplified in a multimode fiber," Light Sci. Appl. **6**(2), e16208 (2016).
9. S. H. Baek and W. B. Roh, "Single-mode Raman fiber laser based on a multimode fiber," Opt. Lett. **29**(2), 153–155 (2004).
10. Y. Glick, V. Fromzel, J. Zhang, A. Dahan, N. Ter-Gabrielyan, R. K. Pattnaik, and M. Dubinskii, "High power, high efficiency diode pumped Raman fiber laser," Laser Phys. Lett. **13**(6), 065101 (2016).
11. E. A. Zlobina, S. I. Kablukov, A. A. Wolf, A. V. Dostovalov, and S. A. Babin, "Nearly single-mode Raman lasing at 954 nm in a graded-index fiber directly pumped by a multimode laser diode," Opt. Lett. **42**(1), 9–12 (2017).

#294679 https://doi.org/10.1364/OE.25.022219
Journal © 2017 Received 27 Apr 2017; revised 20 Jul 2017; accepted 26 Jul 2017; published 5 Sep 2017

Optics EXPRESS

12. B. M. Flusche, T. G. Alley, T. H. Russell, and W. B. Roh, "Multi-port beam combination and cleanup in large multimode fiber using stimulated Raman scattering," Opt. Express **14**(24), 11748–11755 (2006).
13. K. Krupa, A. Tonello, A. Barthélémy, V. Couderc, B. M. Shalaby, A. Bendahmane, G. Millot, and S. Wabnitz, "Observation of geometric parametric instability induced by the periodic spatial self-imaging of multimode waves," Phys. Rev. Lett. **116**(18), 183901 (2016).
14. K. Krupa, A. Tonello, B. M. Shalaby, M. Fabert, A. Barthélémy, G. Millot, S. Wabnitz, and V. Couderc, "Spatial beam self-cleaning in multimode fiber," Nat. Photonics **11**(4), 237–241 (2017).
15. R. Guenard, K. Krupa, R. Dupiol, M. Fabert, A. Bendahmane, V. Kermene, A. Desfarges-Berthelemot, J. L. Auguste, A. Tonello, A. Barthélémy, G. Millot, S. Wabnitz, and V. Couderc, "Kerr self-cleaning of pulsed beam in an ytterbium doped multimode fiber," Opt. Express **25**(5), 4783–4792 (2017).
16. K. Krupa, C. Louot, V. Couderc, M. Fabert, R. Guenard, B. M. Shalaby, A. Tonello, D. Pagnoux, P. Leproux, A. Bendahmane, R. Dupiol, G. Millot, and S. Wabnitz, "Spatiotemporal characterization of supercontinuum extending from the visible to the mid-infrared in a multimode graded-index optical fiber," Opt. Lett. **41**(24), 5785–5788 (2016).
17. L. G. Wright, Z. Liu, D. A. Nolan, M. J. Li, D. N. Christodoulides, and F. W. Wise, "Self-organized instability in graded index multimode fibre," Nat. Photonics **10**(12), 771–776 (2016).
18. Z. Liu, L. G. Wright, D. N. Christodoulides, and F. W. Wise, "Kerr self-cleaning of femtosecond-pulsed beams in graded-index multimode fiber," Opt. Lett. **41**(16), 3675–3678 (2016).
19. C. Michel, M. Haelterman, P. Suret, S. Randoux, R. Kaiser, and A. Picozzi, "Thermalization and condensation in an incoherently pumped passive optical cavity," Phys. Rev. A **84** 033848 (2011).
20. F. El Bassri, F. Doutre, N. Mothe, L. Jaffres, D. Pagnoux, V. Couderc, and A. Jalocha, "Hybrid Q-switched broadband laser source with low timing jitter," Opt. Express **20**(2), 1202–1212 (2012).
21. V. Couderc, A. Crunteanu, M. Fabert, F. Doutre, F. El Bassri, D. Pagnoux, and A. Jalocha, "Picosecond pulse generation in a hybrid Q-switched laser source by using a microelectromechanical mirror," Opt. Express **20**(5), 5524–5529 (2012).
22. N. D. Zameroski, M. Wanke, D. Bossert, "Cavity length dependence of mode beating in passively Q-switched Nd-solid state lasers," Proc. of SPIE **8599**, 85991V (2013).
23. W. Z. Zhuang, M. T. Chang, H. C. Liang, and Y. F. Chen, "High-power high-repetition-rate subpicosecond monolithic Yb:KGW laser with self-mode locking," Opt. Lett. **38**(14), 2596–2599 (2013).

1. Introduction

Multimode optical fibers (MMFs) may provide an interesting alternative to large mode area (LMA) single mode fibers for the fiber-based delivery of high peak power pulses, and for fabricating high-power fiber amplifiers and lasers [1–3]. Indeed, MMFs feature a large effective area, and may be rare-earth doped over their entire core cross-section, without requiring the tight refractive index uniformity and the expensive technology of active LMA fibers. MMFs preserve good guiding properties under bending or thermal load, and their modal instability is reduced when compared with LMA fibers. The main obstacle with the use of MMFs is their inherent degradation of the spatial beam quality leading to modal noise, and, in the short pulse regime, temporal broadening from modal dispersion. Therefore, a control of the output spatial modes and their dispersion is mandatory to ensure the delivery of high quality (brightness) beams and short pulses.

Many techniques have been proposed so far to filter out a given mode (e.g., the fundamental mode) in a MMF amplifier and laser [3-4]. For example, spatial filtering and differential diffraction losses, differential bending losses [1], resonant coupling with a surrounding structure [5], long-period Bragg gratings, tailoring of the doping area [6], and gain guiding [7], to mention a few. Another approach involves adaptive input wavefront shaping by electrooptic phase control in order to properly shape the output beam in spite of the highly multimode propagation environment [8]. Beam self-cleaning resulting from multimode nonlinear propagation provides a potentially much simpler approach for restoring and maintaining a good beam quality throughout a MMF. So far, stimulated Raman scattering (SRS) has been mainly used to demonstrate high brightness MMF amplifiers and lasers, by exploiting Stokes beam cleaning via mode dependent Raman gain [9–12]. Some Raman lasers were even directly pumped by multimode laser diodes [11]. Beam self-cleaning was also recently achieved in GRIN MMFs by exploiting the instantaneous Kerr nonlinearity, which leads to an irreversible power transfer from higher-order modes into the fundamental fiber mode [13–18]. The benefit of self-cleaning is that there is no change to the input light carrier frequency. Significant improvement of the beam quality of sub-nanosecond to sub-

Optics EXPRESS

picosecond pulses at the output of GRIN fibers was demonstrated at multi-kW peak powers. Kerr beam self-cleaning was also recently observed in a Yb-doped MMF amplifier [15]. This suggests its use in a MMF-based laser, for the generation of intense short laser pulses with a quasi-single mode transverse beam profile.

It is interesting to note that in a theoretical work [19] C. Michel *et al.* predicted the existence of spatial phenomena of thermalization and condensation (that is a macroscopic population of the fundamental plane-wave model) of optical waves in passive optical cavities, in the absence of waveguides and with pump pulses whose coherence time is shorter than the round-trip time of the cavity.

In this work we propose and analyze the operation of a new coupled cavity laser, composed by a passively Q-switched Nd:YAG microchip laser and an external cavity comprising an Yb-doped MMF amplifier. Coupled cavity lasers (but enclosing single mode fibers in the external cavity) had been previously used for timing jitter reduction of a Q-switched laser, and for supercontinuum generation [20-21]. Here we show that, by combining functionalities of short and long cavities, one may readily and simultaneously shape the output beam in the spatial, spectral and in temporal domains. We obtained intra-cavity nonlinear beam self-cleaning in the active MMF section under appropriate settings of its gain, and of the coupling between short and long cavities. Moreover, we achieved both Q-switched and Q-switched mode-locked operations, in combination with spatial beam cleaning in the MMF amplifier.

2. Coupled cavity composite laser based on a multimode fiber

Our coupled cavity laser is schematically described in Fig. 1. It is based on a Nd:YAG microchip laser, diode pumped at 808 nm, and passively Q-switched by a thin Cr^{4+} doped YAG crystal. An extended cavity is formed by adding an external high reflectivity mirror M_{ext}, that couples light back into the microchip laser. The coupling strength can be varied by means of a polarizing beam splitter (PBS) interposed between two half-wave plates (HWP).

A 80-cm long section of Yb-doped double clad multimode fiber is inserted in the extended cavity. The Yb-MMF has a diameter of 50 μm, and is characterized by a refractive index profile, which is intermediate between a step and parabolic shape (see inset of Fig. 1). More details on this fiber are provided in Ref [15]. We used two positive lenses (L) to couple light into the MMF, and to collimate the beam at the fiber output. In order to provide extra gain, a multimode beam at 940 nm emitted by a CW pump laser diode (LD in Fig. 1) was injected into the D-shaped (i.e. with a noncircular cross section) double cladding of the MMF through a dichroic beam splitter. The laser diode was equipped with a fiber pigtailed of 200 μm in diameter and a numerical aperture NA = 0.2; the available CW power measured at the output of the pigtail was up to 10 W. The pump field at the output face of the pigtail was then imaged into the input face of the Yb-MMF with a free-space optics system with 1:1 magnification. In a first series of experiments, the pump laser was turned off, and the MMF was operating in the passive regime with or without feedback (i.e. with or without M_{ext}). The results of these studies are reported in section 3. Next, the pump laser was turned on, and the impact of the additional gain provided by the Yb-MMF on the laser operation is discussed in sections 4 and 5. To measure the quality of the laser beam we used a scanning slit beam profiler BC106-VIS combined with an automatic M^2 measurement system (Thorlabs).

Optics EXPRESS

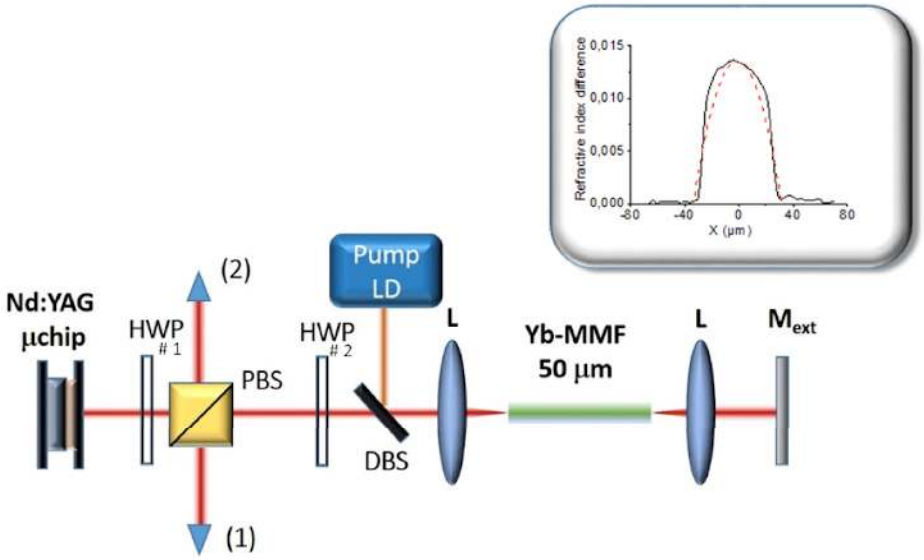

Fig. 1. Schematic of the coupled cavity composite MMF laser comprising a Nd:YAG/Cr:YAG microchip, half-wave plates (HWP), a polarizing beam splitter (PBS), a pump laser diode (LD) coupled to the 80 cm long Yb-MMF by a dichroic beam splitter (DBS) and a highly reflective mirror (M_{ext}). The PBS provides also two of the output ports of the laser, indicated as (1) and (2); a third access point is represented by the weak transmission of mirror M_{ext} Inset: refractive index profile of the fiber core (dark line) compared to a theoretical parabolic profile (Red dashed line).

3. Intracavity nonlinear beam self-cleaning in the MMF of the composite laser

To provide a reference case, we first measured the spatial evolution of the beam delivered by the MMF in a single pass configuration, where the mirror M_{ext} is removed. The uncoupled microchip laser (i.e., in the absence of any reinjected feedback) delivers ~525 ps pulses (see Fig. 2(b)) with a 500 Hz repetition rate, a total average power of 45 mW (maximum peak power: 180 kW), and a beam quality $M^2 = 1.2$. The microchip laser beam was focused on the MMF input facet by forming a spot of nearly 22 μm in diameter. At relatively low input peak power (800 W), the beam observed at the output of the MMF was spatially highly multimode, as illustrated by Fig. 2(a). On the other hand, Fig. 2(c) shows a spectro-spatial analysis of the output field, directly measured by a high-resolution imaging spectroscope, without the additional filtering of a slit. We identified two laser lines separated by ~100 pm, which correspond to two longitudinal modes of the microchip laser with unequal power distribution. Here we may also clearly discern the presence of multiple spatial mode interference: the broad vertical distribution observed at the main wavelength of the microchip laser (see Fig. 2(c)) corresponds well to the spatial dimension of the output transverse pattern of Fig. 2(a).

By increasing the input peak power to about 20 kW, we observed Kerr beam self-cleaning in the 0.8-m long Yb-MMF (here operating in the passive regime). Correspondingly, we observed a strong improvement of the output beam quality, testified by the significant decrease of M^2 from M^2~13 down to $M^2 = 2$. A detailed report on the nonlinear beam evolution of high power sub-nanosecond pulses upon multimode propagation in the same Yb-MMF can be found in Ref [15].

Next, we inserted the cavity mirror M_{ext} to establish a feedback from the fiber cavity into the microchip. It is worth noticing that, due to the large difference in length between the microchip cavity (~7 mm) and the MMF cavity (~1m), and consequently to the large difference in their corresponding free-spectral ranges, there are always resonance frequencies shared by the two cavities, without the need for an electro-optic servo. The multimode

character of the Yb-doped fiber further expands the opportunities for finding common longitudinal modes.

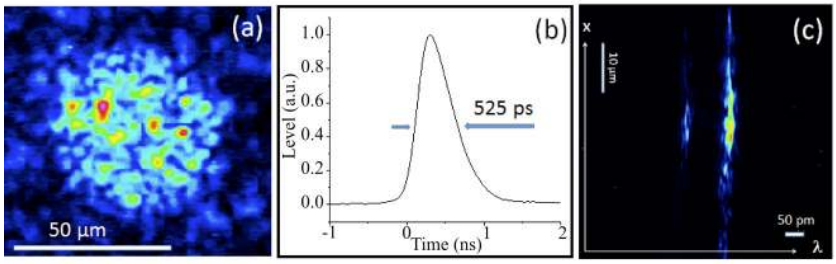

Fig. 2. Characteristics of the output beam after a single pass through the multimode Yb-doped optical fiber, for low input peak power (800 W). Spatial profile (a), temporal profile (b) spectro-spatial analysis (c).

In the linear regime, that is when low power pulses were launched in the MMF, the two cavities were weakly coupled. A highly multimode beam was propagated forward and backward through the MMF. When cavity coupling was sufficiently increased by rotating the half-wave plate #1, we observed the following three signatures of coupled cavity operation: (i) a sudden rise of the power level in the MMF section, which was measured through the leaks of the mirror M_{ext} (~4%); (ii) the excitation of multiple longitudinal modes in the laser spectrum (see Fig. 3(c)); and (iii) a switching by 90° of the polarization orientation of the microchip laser. At the same time, the laser beam at the MMF output, which was monitored through the cavity mirror, switched from a broad speckle pattern to a clean bell-shaped beam.

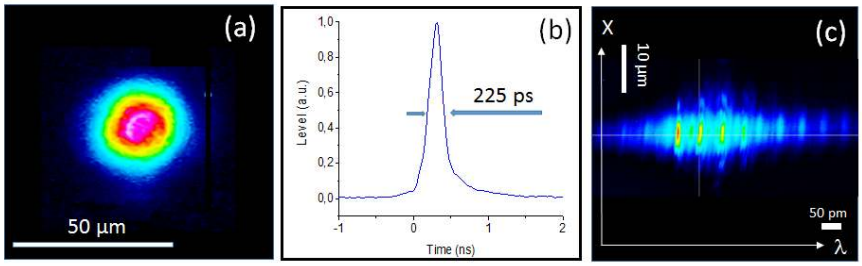

Fig. 3. Characteristics of the output beam measured through the leaks of the M_{ext} mirror obtained in coupled cavity regime at maximum obtained peak power. Spatial profile (a), temporal profile (b) spectro-spatial analysis (c).

A typical example of the obtained self-cleaned beam is shown in Fig. 3(a). The same spatial behavior was observed on the opposite facet of the MMF, imaged through the output (1) of the PBS. The abrupt change in the beam profiles at both ends of MMF was quantitatively confirmed by the measurements of their beam quality, that was significantly improved, with M^2 dropping down to $M^2 = 1.7$. It is interesting to point out that strong cavity coupling preserved Q-switched laser operation with unchanged repetition rate with respect to the uncoupled microchip laser, but the delivered pulses were significantly shortened, with a duration reduced down to 225 ps, see Fig. 3(b) (instead of 525 ps in the absence of coupling, see Fig. 2(b)). Note that, even though the laser pulses are very short with respect to the round-trip time of the extended cavity, their buildup was dramatically affected by feedback coming from the MMF and the mirror.

Optics EXPRESS

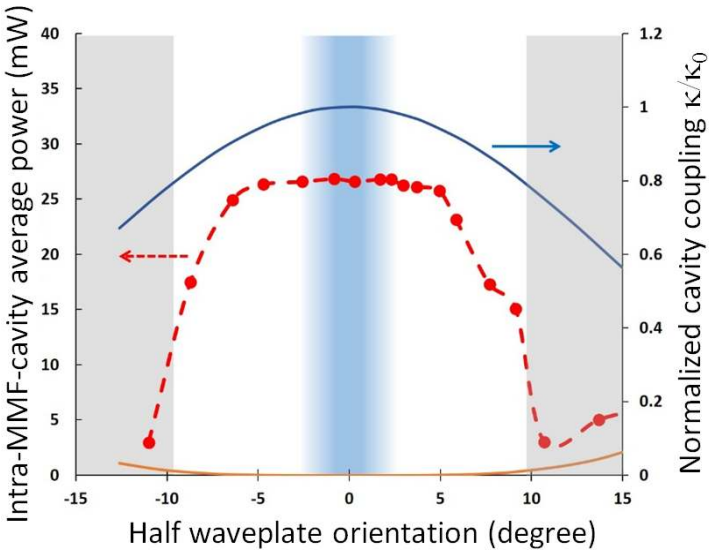

Fig. 4. Intra-cavity average power measured in the MMF branch (red solid dots) for various level of coupling with the microchip cavity, as set by the orientation of the HWP#1. The red dashed line is a guide for the eye. The theoretical normalized cavity coupling is plot in solid blue for p polarization and in orange for s polarization. The grey area gives the boundaries for coupled cavity operation. The central blue area close to zero degrees corresponds to the angular range where mode-beating was observed.

The maximum peak power of pulses circulating in the MMF section of the composite laser cavity was estimated to be close to 200 kW. Port (1) of the PBS provides the major output of the laser, with an average power of about 6 mW. The coupling strength between the two sections of the composite laser cavity, namely between the free-space part and the fiber part, was varied by rotating the HWP#1. Our measurements show that, in order to work in the coupled cavity regime, the HWP orientation should be included in a 20° angular range (see Fig. 4), which corresponds to a situation of strongest reflection of the extended cavity back into the YAG laser. We can estimate that the coupling coefficient between the small and long cavity κ, normalized to its maximum value κ_0, is directly dependent on the HWP orientation θ. For the polarization state (p) transmitted by the PBS we have $\kappa/\kappa_0 = \cos^4(2\theta)$, whereas for the polarization state (s) reflected by the PBS we have $\kappa/\kappa_0 = \sin^4(2\theta)$. In the range where the intra-cavity field in the fiber section remained at a nearly constant high level (~25 mW), nonlinear beam self-cleaning was well maintained. Whereas, self-cleaning disappeared when the coherent coupling was lost, *i.e.,* outside the limit angles $\theta = \pm 10°$.

4. Nonlinear beam self-cleaning with gain in the Yb-MMF

Next, we switched on the pump laser at 940 nm, in order to change the Yb-MMF into an amplifier. However, before turning on the pump radiation, we revised the setting of the fiber cavity, in order to reduce the intra-cavity power by introducing new losses thanks to the HWP#1. The Yb-MMF gain could be varied with the pump power, up to a maximum of G = 23 (when measured for an input signal of 0.5 kW peak power [15]). The available amplifier gain was however limited by the damage threshold of the fiber end face. The fiber damage is likely to be facilitated by the inhomogeneous distribution of dopants along the fiber. The main impact of MMF gain was an increase of the output laser power, and the addition of an ASE background to the output beam pattern, owing to the low pulse repetition rate fixed by our laser system. An example of the output beam registered at the maximum gain condition is shown in Fig. 5(a). The beam pattern was still quasi bell-shaped, and similar to the

Optics EXPRESS

fundamental mode. However, the beam profile was not as clean and perfectly circular as in the passive MMF situation. The corresponding laser spectrum exhibits a discrete structure including the longitudinal modes fixed by the coupled cavities (see Fig. 5(c)). The beam quality remained high with M^2 = 1.8, as measured on the leaks of the M_{ext} mirror. The temporal profile (see Fig. 5(b)) of the output pulse was close to that obtained in the absence of fiber gain. However, the temporal profile exhibited a more asymetric shape, with a 350 ps duration (FWHMI). Such Q-switched mode was reproducible with peak power fluctuations of less than 10%, despite the weak temporal modulations appearing on the pulse profile (see Fig. 5(b)).

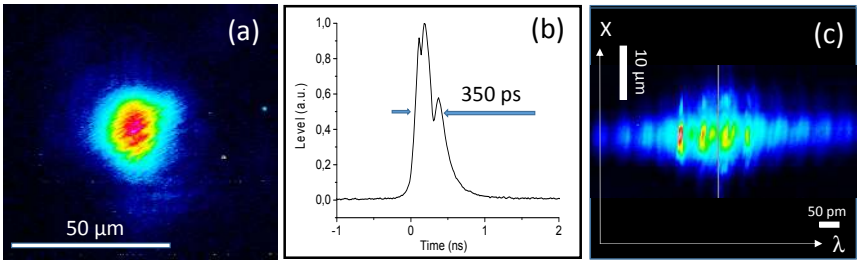

Fig. 5. (a) Laser beam image recorded at the output M_{ext} mirror at the maximum output peak power; (b) Temporal shape of the Q-switched pulse; (c) Spectro-temporal analysis of the output beam.

For a complete characterization of our coupled cavity laser, we measured the average output power at all three available output ports of the composite laser. Namely, after the M_{ext} mirror, and at the two ports of the PBS. Maximum output power is obtained by properly adjusting the level of losses introduced by the PBS when light travels back toward the microchip, after a round-trip in the extended fiber cavity (output (1), Fig. 1). Almost 10 mW of average power (Fig. 6) was obtained with 500 Hz repetition rate and pulse durations close to 300 ps. The output power increase due to the presence of the active fiber is only moderate (we have obtained 6 mW with the unpumped MMF). However, one should bear in mind that, in order to avoid damaging the MMF, extra losses had to be added in the extended cavity. The estimated output peak power reached 66 kW. A second laser output was provided by the residual transmission of the extended cavity rear mirror M_{ext}. In that position, we measured 2.2 mW (which corresponds to 14 kW of peak power). The third output port was provided by the leakage of light coming out from the microchip before the fiber (output (2), Fig. 1). Such power, which was due to the PBS, remained clamped to a value below 0.2 mW.

5. Q-switched mode-locking and intracavity nonlinear conversion in the active Yb-MMF

For particular settings of the HWP#1, close to its orientation at 0°, we observed significant changes in the output pulse temporal profile: Q-switched pulses became strongly modulated in time, leading to a train of pulse bunches. The bunch envelope remained within the same range of 300-400 ps durations and profiles (see Fig. 7) as within the smooth Q-switched pulses observed in previous situations. However, in the pulse bunch case, each sub-pulse was of less than 50 ps duration (limited by our 20 GHz detection chain), with 85 ps temporal spacing. The corresponding repetition rate is consistent with the roundtrip time of the microchip cavity: therefore, the short pulses may result from a beating among longitudinal modes of the microchip laser or a partial mode-locking (ML) effect, since the modulation depth of the pulse train was measured to be 72% within the Q-switched pulse. The bunch train operating regime was not as stable as in the previous cases: through long acquisitions with the oscilloscope (in the segmented memory option) we observed some long-term fluctuations. Moreover, we identified that the partial ML or mode-beating behavior is not

Optics EXPRESS

connected with beam propagation in the MMF: rather, ML is a consequence of the extended cavity feedback. In fact, even when removing the MMF we still observed Q-switched self-mode-locked pulses, similar to those in Fig. 7(a). Such ML effect was previously discussed in the literature, and explained as either resulting from the dynamics of coupled cavities, or from nonlinear spatial beam reshaping in a multimode microchip [22-23].

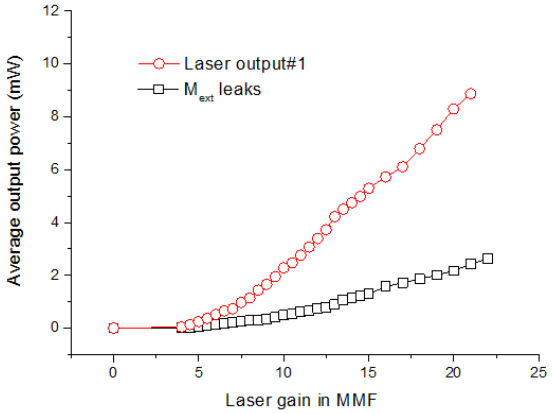

Fig. 6. Average output power of the Q-switched composite laser as a function of gain in the MMF.

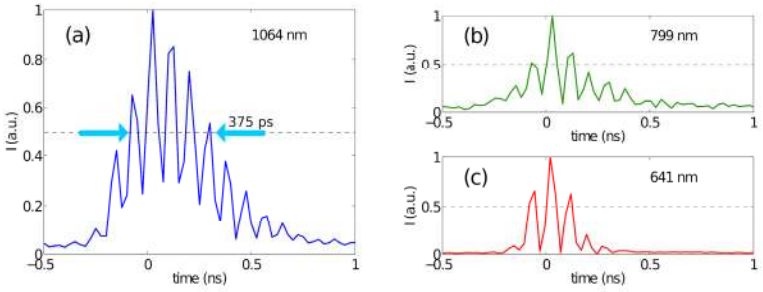

Fig. 7. Temporal profile of the Q-switched mode-locked pulses at: 1064 nm (a); 799 nm (b); 641 nm (c).

The ML regime permitted to reach higher peak intensities, so that nonlinear frequency conversion occurred in the MMF. Remarkably, new frequency generation was accompanied by the formation of bell-shaped beams at those frequencies. New frequencies were generated by four-wave-mixing, an effect that was not observed in all previously mentioned coupled-cavity experiments. Our laser produced sharp anti-Stokes components at 641 nm (AS2) and at 799 nm (AS1), along with their Stokes counterparts at 1592 nm (S1) and presumably at 3128 nm (S2), which is out of the reach of our spectrum analyzer (see Fig. 8(a)). The corresponding temporal profiles at these sidebands have a much higher modulation depth, as reported in Figs. 7(b) and 7(c). The associated frequency detuning from the pump beam is 93 THz and 186 THz for AS1 and AS2, respectively. All wavelengths obtained in the visible and near infrared domains essentially propagate in the fundamental mode, and exhibit a quasi-Gaussian beam shape (see Figs. 8(b), 8(c), 8(d)). Spectral powers carried by these new spectral lines are 11 dB below the pump level at 1064 nm.

It was previously demonstrated that temporal modulation instability, induced by the periodic spatial self-imaging of a multimode beam (or geometric parametric instability (GPI)), may produce sideband peaks with a very large detuning in normal dispersion regime

Optics EXPRESS

[13]. That result was obtained in a graded-index MMF, where propagation constants of the guided modes are equally spaced. In our case, the refractive index profile of the fiber core departs from a parabolic law, a situation which is known to be less favorable to spatially periodic self-imaging. Nevertheless, the observed four-wave mixing processes provide a spectral signature of GPI, resulting from a multimodal nonlinear parametric interaction. In fact, as a first approximation, if we consider a relative index difference of 9.5×10^{-3}, a core diameter of 50 µm, and an estimated dispersion of the Yb-MMF of −50 ps/(km nm), the frequency detuning of the first sideband is expected at 96.5 THz, which agrees fairly well with the experimental results. Moreover, the laser gain saturation could reinforce the modulation depth of a weakly efficient periodic self-imaging process.

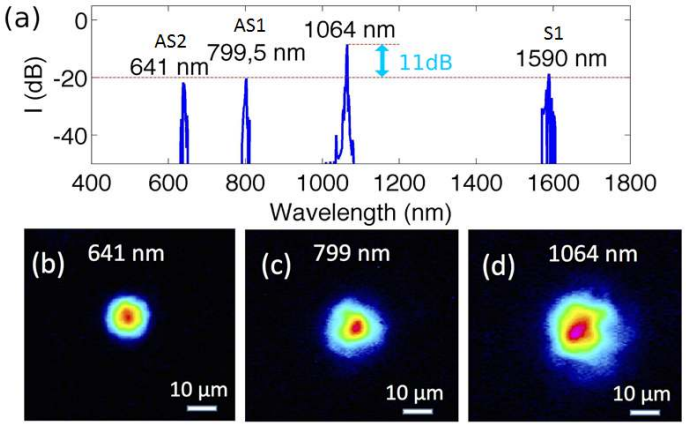

Fig. 8. (a) Laser beam image recorded behind the output M_{ext} mirror; Output spectrum of the laser for the HWP# 1 oriented close to 0°. The mode-locked regime leads to FWM generated with far detuned spectral lines.

Conclusion

We demonstrated Q-switched, and Q-switched mode-locked operation of a composite laser comprising a Nd:YAG microchip laser and a Yb-doped multimode fiber in an extended cavity. For a sufficient coupling strength, beam self-cleaning was obtained in the MMF, thanks to nonlinear mode coupling. Spatial quasi-single mode operation (M^2 = 1.8) was demonstrated at 1064 nm, with output pulses exhibiting peak powers higher than 66 kW in the active configuration. For some particular polarization settings, the composite laser delivers short pulse trains (Q-switched and mode-locked) with even higher peak intensity. This regime gives rise to intra-cavity nonlinear frequency conversion in the active MMF through GPI. Far detuned sidebands in the visible and in the near infrared domains were observed, with frequency detuning of 93 THz and 186 THz.

Funding

Horiba Medical and BPI-France in the frame of the Dat@diag project (Industrial Strategic Innovation Program); Région Limousin (C409 SPARC); Italian Ministry of University and Research (MIUR) (Ministero dell'Istruzione, dell'Università e della Ricerca (MIUR) (PRIN 2015KEZNYM); Ministry of Education and Science of the Russian Federation (Minobrnauka) (14.Y26.31.0017); European Union's Horizon 2020 research and innovation programme under the Marie Skłodowska-Curie grant agreement No 691051.

Acknowledgment

In particular, the work of Stefan Wabnitz was supported by Minobrnauka. All Authors have equally contributed to this work.